Carcinogenesis vol.21 no.7 pp.1411–1421, 2000

Quantitative analysis of tumor initiation in rat liver: role of cell replication and cell death (apoptosis)

Bettina Grasl-Kraupp[3], Georg Luebeck[1], Alexandra Wagner, Alexandra Löw-Baselli, Mathisca de Gunst[2], Thomas Waldhör, Suresh Moolgavkar[1] and Rolf Schulte-Hermann

Institut für Krebsforschung der Universität Wien, Borschkegasse 8a, A-1090 Vienna, Austria, [1]Fred Hutchinson Cancer Research Center, Public Health Sciences Division, MP-665, 1124 Columbia Street, Seattle, WA 98104, USA and [2]Department of Mathematics and Computer Science, Free University of Amsterdam, De Boelelaan 1081, 1081 HV Amsterdam, The Netherlands

[3]To whom correspondence should be addressed
Email: bettina.grasl-kraupp@univie.ac.at

The formation and development of initiated cells has been studied at the beginning of hepatocarcinogenesis. Rats received the genotoxic carcinogen *N*-nitrosomorpholine (NNM); placental glutathione *S*-transferase was used as a marker of initiated cells (G+ cells). Single G+ cells appeared within 24 h after NNM; their frequency increased steeply for ~2 weeks, then decreased and finally remained constant. G+ foci consisting of ≥2 G+ cells appeared successively after the single cells. Histological determination of DNA replication and apoptosis revealed that: the formation of single G+ cells may not depend on DNA replication of precursor cells; single G+ cells showed considerably lower DNA replication than G– normal hepatocytes; from the 2-cell stage onwards G+ foci displayed enhanced DNA replication and apoptosis. Data from histological sections were transformed into the third dimension by a new stereological method which considers the non-spherical shape of many G+ lesions. Rates of division and death of G+ cells and of formation and growth of G+ foci were estimated by a stochastic model: initially G+ clones appeared at a rate of 12 000 per day and liver until a maximal number of 176 000 (phase I) was reached; thereafter they declined to 134 000 (phase II); they then remained constant (phase III). Estimated division rates of G+ cells decreased from phase I to phase III, while the death rate increased in phase II, when every third G+ clone disappeared. As a result, at day 50 after NNM only 0.3% of G+ single cells had formed a clone containing ≥5 cells. In conclusion, experimental and computed parameters provide direct evidence that hepatocarcinogenesis evolves clonally and that initiated hepatocytes have a selective proliferation advantage, associated with an enhanced potential to undergo apoptosis. Thereby, depending on the conditions, initiated clones expand or become extinct. Extinction may lead to reversion of the biological effects of initiation.

Abbreviations: 2D, two-dimensional; 3D, three-dimensional; AB, apoptotic body; AI, apoptotic body index; CI, confidence interval; G+, placental glutathione *S*-transferase-positive; G–, placental glutathione *S*-transferase-negative; GLDH, glutamate dehydrogenase; GST-P, placental glutathione *S*-transferase; LI, labeling index; NNM, *N*-nitrosomorpholine.

Introduction

Initiation is a key event in carcinogenesis. The operational definition of initiation implies that it renders a cell prone to clonal growth under the influence of promoters and that this change is persistent and is passed on to subsequent generations of cells (1–3). Because initiation is a rare event affecting only a few cells within a tissue and because in most models no specific markers for initiated cells are available, direct investigation is difficult. Therefore, the biological and molecular properties of initiated cells and of their immediate successors are not well understood. Qualitative and quantitative characterization of initiation would be of great value to understand chemical carcinogenesis and to design cancer prevention strategies.

In rat liver the expression of placental glutathione *S*-transferase (GST-P) is a useful marker for most (pre)neoplastic lesions (4,5). Studies on the very first stages of hepatocarcinogenesis have become feasible after the discovery of selective staining of single rat hepatocytes for GST-P [placental glutathione *S*-transferase-positive (G+) and placental glutathione *S*-transferase-negative (G–) cells], which appear after administration of various genotoxic hepatocarcinogens, but not after tumor promoters and other non-genotoxic agents (6). Formation of G+ single cells increased with the dose of the genotoxic initiator and decreased when metabolic activation of the initiator to the ultimate carcinogen was inhibited (6–8). Mutated Ha-*ras* was found in small preneoplasias of mice and rat liver a few weeks after initiation, suggesting that the mutation occurred early in the carcinogenic process (9,10). Furthermore, the incidences of single cells with the G+ phenotype or with a mutation in the albumin locus were nearly identical, which supports the hypothesis that the formation of G+ cells results from a mutational event (11). When initiation is followed by treatment with a tumor promoter a small percentage of G+ single cells develop to G+ foci, which may give rise to G+ tumors (6,12). Based on these findings, most investigators assume that single G+ hepatocytes are initiated and capable of evolving into hepatic neoplasia.

The number of initiated cells within an organ is a major determinant of the risk of cancer formation. In previous studies the dose of the initiating carcinogen, extent of genotoxic damage, size or frequency of putative preneoplastic liver foci and incidence and multiplicity of tumors have been used as the main parameters of mathematical models developed for the description and prediction of carcinogenesis (13–20). In the present work a quantitative analysis has been performed on the formation and further fate of G+ single cells using both experimental and mathematical methods. To compute the number and the three-dimensional (3D) size distributions of G+ lesions we first applied stereological procedures, used in previous studies (21–23). However, these procedures assume a spherical shape of preneoplasias, a condition not met by many small G+ lesions. Therefore, a novel stereological approach was developed and used that is based on a discrete

computer model for the variable 3D aggregation of G+ cells into lesions (24; E.G.Luebeck and M.de Gunst, manuscript in preparation). Combined with a temporal stochastic growth model for these lesions it allows for the quantitative estimation of the number and sizes of clones (i.e. the number of G+ single cells, of G+ foci and of G+ cells within foci) in the liver as a function of time (16,25). The parameters of the growth model are estimated from transectional observations; they provide quantitative information on the rate of initiation as well as of division and death of G+ cells, which can be determined only partly from experimental observations. Thus, model-derived estimates are essential for understanding the cell kinetics of initiated cells in the first period after carcinogenic insult.

The crucial property of initiated cells is considered to be their potential for selective growth under the influence of growth-promoting stimuli. Whether this property is acquired during initiation and is already expressed by single initiated cells has not been investigated experimentally. Studies on more advanced stages of hepatocarcinogenesis revealed that preneoplasias and neoplasias exhibit higher replicative activities than normal liver, leading to preferential expansion (26–28). Apoptotic activity also increases from normal liver, to foci, to adenomas and to carcinomas (27,29). As a result, cell turnover is accelerated in the course of hepatocarcinogenesis. However, at all stages rates of cell replication were higher than those of apoptosis, allowing a net gain of (pre)neoplastic cells (27,29). Tumor promoters suppress apoptotic activity and thus further accelerate growth of the lesions. In the case of withdrawal of the promoter, the high rate of apoptosis in (pre)neoplasias may increase even further, leading to a net loss of cells and to selective regression of tumors and tumor prestages while the surrounding unaltered tissue is little affected (27,29–31).

To study the growth characteristics of the very first stages of hepatocarcinogenesis we applied *N*-nitrosomorpholine (NNM), one of the nitrosamines occurring in tobacco smoke and in a variety of foods and alcoholic beverages, which likely contributes to the development of human cancer (32,33). NNM causes damage to and death of hepatocytes, activation of p53, inflammation, regeneration of the liver and, finally, the development of numerous preneoplastic lesions that evolve into tumors under various promoting stimuli (34–37). Similar events are associated with human hepatocarcinogenesis. Therefore, NNM-induced changes may provide a useful model to elucidate the mechanisms of carcinogenesis in the mammalian liver.

In the present study application of NNM generated numerous G+ single cells in the livers of rats; a subfraction of these cells developed into larger clones. In single G+ cells replication was low but in G+ mini-foci replication and death of cells were increased. This indicates that the defects in growth control, previously found in more advanced (pre)neoplasias, are acquired during initiation or soon thereafter and become manifest in the first stages of carcinogenesis. These studies provide direct experimental evidence that initiated cells have a selective growth advantage. In addition, their increased rate of apoptosis suggests the potential to undergo selective elimination. By this mechanism clones carrying the irreversible 'initiation effect' may become extinct under certain conditions. This would lead to reversal of the biological effects of initiation.

Materials and methods

Experimental studies on early hepatocarcinogenesis

Animals and treatment. Male SPF Wistar rats, 3–5 weeks old, were obtained from the Zentralinstitut für Versuchstierzucht (Hannover, Germany). Animals were randomly assigned to experimental groups, kept under standardized conditions (Macrolon cages, 20 ± 3°C room temperature, 40–70% relative humidity) and fed Altromin 1321N (Altromin, Lage, Germany). After 3 weeks adaptation animals were treated with NNM (Serva, Heidelberg, Germany); immediately before application, NNM was dissolved in phosphate-buffered saline, pH 7.4, and was given as a single dose of 250 mg NNM/10 ml solution/kg body wt by gavage between 8 and 9 p.m. when the wave of hepatic DNA synthesis was at its peak (see below). Controls were treated with pure solvent only. Unless otherwise stated, [^{3}H]thymidine (6.7 Ci/mmol; NEN, Frankfurt, Germany) was injected into the peritoneal cavity as a single dose of 0.2 mCi/kg body wt between 8 and 9 p.m. Thirty-six hours later animals were killed by decapitation under CO_2 narcosis. For more detailed descriptions see Grasl-Kraupp *et al*. (27). The experiments were performed according to the Austrian guidelines for animal care and protection.

Four animals each were analyzed at days 0.5, 1.5, 2.5, 17.5, 20.5, 24.5, 27.5 and 31.5 post-NNM treatment; the number of animals analyzed at days 0, 3.5, 4.5, 7.5, 13.5 and 107.5 were 9, 6, 2, 3, 3 and 10, respectively.

The determination of hepatic DNA content was as given elsewhere (38). The extent of cell lysis was estimated by determining serum glutamate dehydrogenase (GLDH) activity, applying commercial test kits (Merck, Darmstadt, Germany).

Histology and morphology. Liver weight was recorded and specimens of liver tissue were fixed and processed as described (27). Sections 2 µm thick were stained either with hematoxylin and eosin or by immunohistochemistry, which was accomplished by the unlabeled antibody peroxidase–anti-peroxidase technique according to previous descriptions (39). The following antisera were used (dilutions in parentheses): anti-GST-P (1:320) (Biotrin International, Dublin, Eire); anti-rabbit immunoglobulin and horseradish peroxidase–anti-peroxidase complex (both 1:50) (Dakopatts, Glostrup, Denmark). G+ single cells and G+ multicellular foci were identified by the anti-GST-P stain. Autoradiography for evaluation of labeling indices was performed as described (27).

For 3D reconstruction of G+ single cells 30 serial sections, 4 µm thick, were stained for GST-P and subjected to autoradiography. Any G+ single cells, with or without [^{3}H]thymidine label, were identified in serial section no. 15. Individual G+ cells were then followed in the consecutive serial sections (nos 16–30 and 14–1) using two microscopes linked by a bridge for overprojection (Zeiss, Germany). Whether a G+ single cell was actually single or whether there was immediate contact with one or more G+ cells in one of the serial sections was recorded. This allowed 3D reconstruction of the actual size of lesions of 1, 2 or >2 G+ cells.

Areas of evaluated tissue sections or areas of necrotic liver tissue were measured by means of a semi-automatic image analyzer (VIDS IV; Ai-Tektron GmbH, Meerbusch, Germany).

Experimental determination of DNA synthesis and of apoptosis per day. Implantation of osmotic minipumps may lead to significant shifts in proliferation kinetics in liver regenerating after toxic injury (W.Bursch, personal communication). We therefore used the following protocol that allows for the determination of rates of cell replication and apoptosis per day. Animals were adapted to rhythmic feeding (from 9 a.m. to 2 p.m.) from 4 weeks before NNM treatment until the end of the experiment. This procedure synchronizes DNA synthesis and, presumably, apoptosis in unaltered liver and in preneoplastic lesions to single waves per day, which are ~12 h apart (27,40). At the peak of DNA synthesis, replicating cells were labeled by [^{3}H]thymidine application. In order not to disturb their eating behavior, animals were killed 36 h later, allowing determination of apoptosis at its daily maximum.

Determination of cell replication. The labeling index (LI) is defined as the number of labeled nuclei/100 nucleated hepatocytes; LIs were determined in at least 2000 hepatocyte nuclei/liver and in all nucleated cells of individual G+ cell clones.

We assumed that all labeled hepatocytes proceeded through mitosis, as shown previously (41). We tested whether or not a fraction of labeled hepatocytes underwent a second cell division during the 36 h interval between [^{3}H]thymidine application and death. [^{3}H]thymidine was injected 24 h post-NNM; there was no significant difference between the LIs of animals killed either 12 [9.43, 95% confidence interval (CI) 8.82–10.1] or 36 h later (10.56, 95% CI 9.98–11.2) and hence no evidence for a second replication cycle within 36 h.

To study whether rhythmic feeding synchronizes DNA synthesis of G+ single cells, as shown for (pre)neoplastic lesions (27,40), a subgroup of four animals received three consecutive injections of [^{3}H]thymidine at 1, 6 and

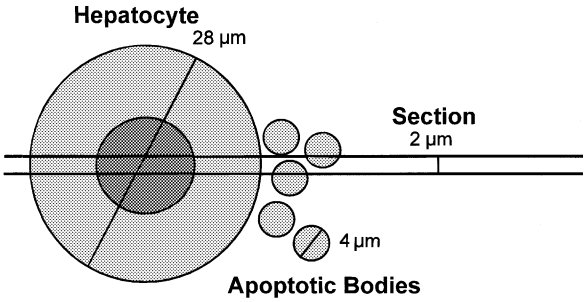

Fig. 1. Different probabilities that an intact hepatocyte and an apoptotic body are cut in a tissue section.

11 p.m on day 19 post-NNM treatment. The percentage of labeled nuclei of G+ single cells obtained with this protocol was 2.2% (95% CI 0.46–6.38), as opposed to 1.94% (95% CI 0.5–4.96) after a single injection at 8 p.m. This result indicates that rhythmic feeding also synchronizes DNA synthesis of G+ single cells.

Determination of cell death by apoptosis. Apoptotic bodies (ABs) were identified in hematoxylin and eosin stained sections according to previously established criteria (30). The apoptotic body index (AI) indicates the number of ABs per 100 intact hepatocytes. AIs were determined in >4000 unaltered cells/liver, in all cells of individual G+ clones and in all unaltered cells immediately surrounding G+ cells.

In untreated livers of full-grown rats with balanced gain and loss of hepatocytes, LI is on average ~3-fold higher than AI (27,40). In order to estimate the actual loss of hepatocytes per day we multiplied the AI by a correction factor of 3. The discrepancy between LI and AI was expected for the following reasons. ABs and hepatocytes are of approximately spherical shape with a mean diameter of 4 and 28 µm, respectively, as schematically depicted in Figure 1 (W.Bursch, personal communication; 42). According to Fullman's formula the relative probability of cutting hepatocytes and ABs in a section 2 µm thick is $(4 + 2)/(28 + 2) = 0.2$ (21); thus the probability of detection is 5-fold lower for ABs than for hepatocytes. Furthermore, one hepatocyte undergoing apoptosis usually breaks into several ABs, which are supposed to be randomly grouped in three dimensions; in two dimensions two ABs are seen on average. In summary, the probability of finding at least one residue of a dying hepatocyte may be lower by a factor of 2–3 than of seeing an intact hepatocyte.

The detection of GST-P is not reliable in dead cells; false negative and false positive ABs can be observed (not shown). Therefore, it is unclear whether an extra- or intracellular AB in the immediate surroundings of a G+ cell derives from a normal G– hepatocyte or from a second G+ cell. To overcome this problem, we counted ABs, independent of their staining pattern for GST-P, within G+ foci and in the immediate surroundings of G+ cells (m). Thereafter the estimated 'background' number of ABs deriving from unaltered G– hepatocytes was subtracted from m using the following formula:

$$\mathrm{AI}_{\mathrm{corr}} \text{ for G+ cells} = 3\times\{(m - a)/N_{\mathrm{G+}}\times 100\}$$

m is the number of ABs within G+ cells and in hepatocytes immediately surrounding G+ cells, $a = N_{\mathrm{surr}}\times \mathrm{AI}_{\mathrm{unalt}}/100$, N_{surr} is the number of hepatocytes immediately surrounding G+ cells, $\mathrm{AI}_{\mathrm{unalt}}$ is the index of ABs in unaltered G– hepatocytes and $N_{\mathrm{G+}}$ is the number of G+ cells.

Modeling growth and regression of G+ single cells and multicellular foci

The clonal growth model. The G+ cell clones observed in this experiment were analyzed quantitatively via a stochastic growth model which provides explicit expressions for the number and size distributions of the clones. To be specific, let X be the number of normal hepatocytes that are at risk of acquiring the G+ phenotype. This alteration may occur either spontaneously or in response to genotoxic exposures such as the NNM exposure described in the present experiment. Let v be the rate (per cell) at which normal hepatocytes are transformed into G+ cells. Clones are then assumed to arise according to a non-homogeneous Poisson process with rate vX. In the context of chemical carcinogenesis this process is referred to as initiation. Subsequent clonal expansion of the initiated cells is described in terms of a simple birth and death process. Initiated cells either divide with cell division rate α or disappear with rate β. The model, however, does not distinguish between cell loss due to apoptosis and loss of the G+ enzyme marker. Only cells or clones of cells that show the G+ phenotype are evaluated by the mathematical analyses here.

Based on these assumptions formulae for the number and size distribution of initiated cells were derived by Dewanji *et al.* (16) and are explicitly evaluated here for the case of piecewise constant parameters assuming (mean) exponential growth of the clones (see Appendix).

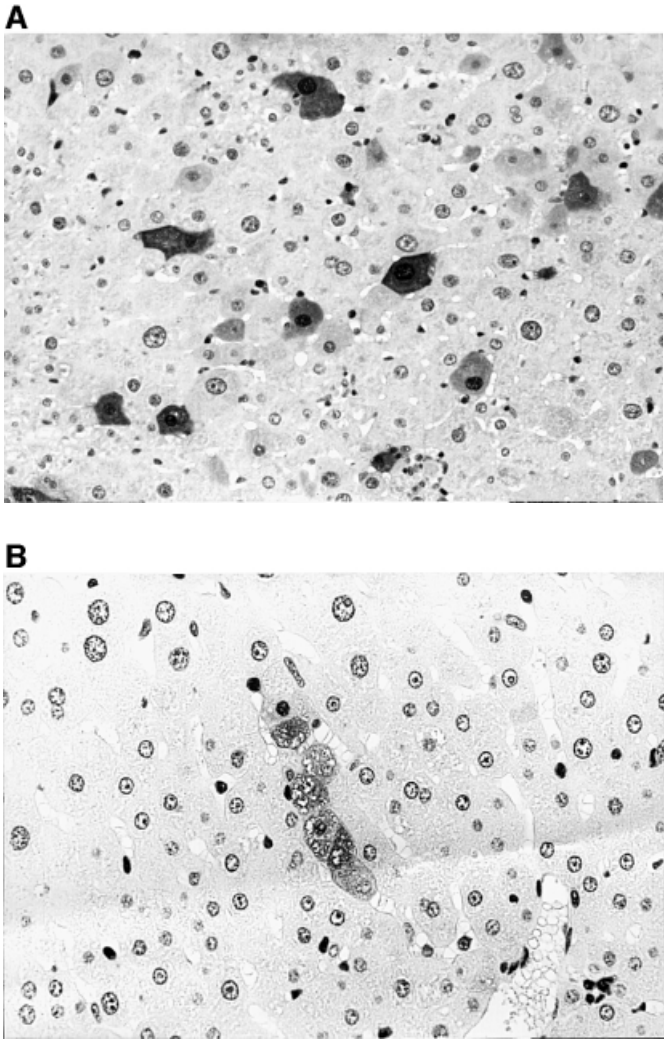

Fig. 2. G+ single cells and multicellular foci in rat liver 7.5 days after NNM treatment. (**A**) Numerous G+ single cells randomly distributed within a liver lobule. (**B**) A G+ focus consisting of six cells configurated as a row. Magnification ×125.

Stereology. Several analytical methods are available that deal with the stereological problem, namely the problem of how to translate the number and size distribution of foci seen in two-dimensional (2D) tissue sections to the respective 3D quantities. Most parametric methods (i.e. methods that assume a parametric form of 3D size distribution like the clonal growth model described above) assume that foci are of spherical shape, an assumption that is clearly inadequate for small foci such as those observed in this experiment (see Results and Figure 2). In order to address this problem a discrete stereological method was used that deals with the stereology of randomly shaped cellular clusters and was applied to a subset of the data presented in this study (for details see ref. 24). By analogy with Wicksell (43) and the Saltykov method (22) for spheres this method consists of a discrete 3D to 2D transformation.

However, in contrast to these methods, this new method is applicable to other shapes than spheres and the sizes of the observed transections are given in terms of the number of transected cells rather than in terms of radii or areas. The Saltykov-like coefficients, here referred to as a_{nm}, represent the probabilities of transecting an arbitrary clone of size m and observing n cells per unit area in the transection. These coefficients were obtained by simulating the random spatial configurations of small cell clusters composed of tightly packed cuboidal cells. They do not depend on the parametric growth model, but only on the possible spatial configurations of the clones. The computer simulations used to generate the coefficients a_{nm} are based on cellular parameters that define the random configurations of cells within the clones. The specific cellular parameter used here has been described in detail (24;

E.G.Luebeck and M.de Gunst, manuscript in preparation) and was selected to closely reflect the observed clone assemblies in rat liver while preserving computational simplicity.

Our analyses were restricted to foci showing no more than 20 cells. Two separate calcluations were performed. The first without a lower limit ($n \geqslant 1$) and the second with a lower size limit ($n \geqslant 2$). For computation of the transformation coefficients a_{nm} an upper size limit of $M = 200$ cells was selected.

Hepatocytes are described as densely packed cubes of fixed length. We chose $a = 28$ µm, a value that is close to that derived from the measured mean cellular volume of focal hepatocytes (42). For completeness, we provide the relevant expressions for analysis of the 2D data observed in this experiment.

Let the size distribution p_m represent the probability that a clone which is observed at time t contains m cells. Since we assume an upper size limit at $M = 200$ cells, $p_m = 0$ for $m > M$. Time of origin of the clone is integrated out. The number of non-extinct clones in a unit volume at time t, N_V, is Poisson distributed with mean Λ. We note that p_m, N_V and Λ and all quantities derived from them depend on t. For simplicity, we omit this dependence in our notation. The expressions for p_m and Λ are derived in the Appendix.

The conditional probability q_n of finding a transection that shows exactly n ($\leqslant$20) cells at time t is given by

$$q_n = (\sum_{m=n}^{M} a_{nm} p_m)/EZ,\ n = 1,\mathrm{K},\ M$$

with the denominator defined as

$$EZ = \sum_{n=1}^{M} \sum_{m=n}^{M} a_{nm} p_m.$$

Assuming that the clones are Poisson distributed in space, the number of transections observed at time t on a section of area A, N_A, is also Poisson distributed with mean $EN_A = A\Lambda_V EZ$.

Likelihood maximization. We fitted the model to the data by maximizing the likelihood with respect to the model parameters α, β and vX on each of several time intervals, starting at the time of birth. The time intervals were selected to partition the entire period from birth of the animals to 51 days after NNM so that important changes in the initiation rate and cell kinetic parameters could be adequately captured. It is important that the time origin is chosen to coincide with the birth of the animal since foci may occur spontaneously prior to NNM exposure at day 56. Preliminary analyses, using up to four different time intervals with variable change points, showed that a partitioning of the time line into three intervals post-NNM was adequate to fit the data.

Phase I: expansion phase from 0 to 14 days after NNM.
Phase II: regression phase from 14 to 28 days after NNM.
Phase III: stabilization phase from day 28 after NNM onwards.

The likelihood of the data is given by a product of the probabilities over all sectional observations, i.e.

$$L = \prod_{i \varepsilon \text{ sections}} [\text{Poisson}\,(N_{Ai}) \prod_{j=i}^{N_{Ai}} q_{nij}],$$

where the index i runs over all sections observed, their area being A_i, and where n_{ij} denotes the number of cells seen on the jth transection of the ith section.

The likelihood was maximized using the DFP algorithm (44) and confidence intervals were obtained using the profile likelihood method (45). As will be illustrated in the next section, the results, using the maximum likelihood estimates, can either be expressed in terms of 3D quantities (size distribution, expected number of 3D clones per ml liver) or in terms of observable 2D quantities.

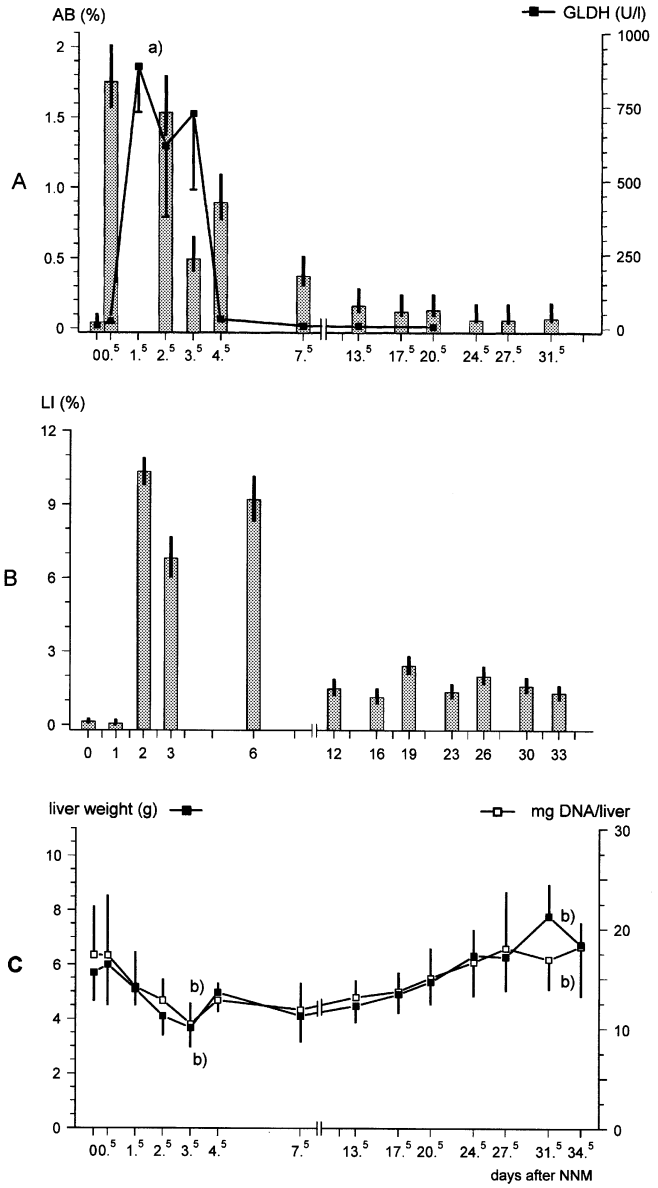

Fig. 3. NNM-induced effects in the liver. (**A**) Incidence of apoptotic bodies (AI%) in G– hepatocytes at the time point of killing is given by the columns. The black line represents the serum activity of GLDH and is expressed as means ± SEM. (**B**) Incidences of replicative DNA synthesis (LI%) in G– hepatocytes are given at the time point of [^{3}H]thymidine application. (**C**) The effect of NNM treatment on absolute liver weight and hepatic DNA content (means ± SD). In (A) and (B) no overlap of vertical lines indicates significance at the 95% level. In (A) and (C) significance of differences of means was calculated by the Rang test: $^aP < 0.001$; $^bP < 0.05$ (calculated separately for days 0–3.5 and 3.5–34.5 post-NNM treatment).

Results

NNM effects on survival, daily food intake and on body and relative liver weights

Two of 150 rats died within 1 week after NNM application. Thereafter no further loss of animals occurred until termination of the experiment. Immediately after treatment food intake was reduced from ~16 to ~2 g/day/animal. Subsequently food consumption gradually recovered and reached its initial amount 10 days after NNM. NNM-treated animals showed maximal loss of body weight on day 5 (115 ± 16 versus 159 ± 9 g, $P < 0.001$ according to Wilcoxon's test), which returned to pretreatment levels within 25 days.

NNM-induced loss of liver tissue

After NNM application a wave of apoptosis occurred at the 12 h time point (Figure 3A). This was followed by the appearance of large areas of hepatocellular necrosis around the central venules at 24 h (not shown). Morphometric analysis at the maximal extension of damage 36 h after NNM demonstrated that 45 ± 7.9% of total liver area was affected by necrosis. On the border of the necrotic areas liver cell death

through apoptosis was detected. Due to massive damage of the liver tissue a thorough quantification of apoptotic bodies at the 36 h time point was not feasible.

Determination of GLDH activity in the serum revealed an at least 100-fold elevated activity ~48 h after NNM application and a steep decline to basal levels within the following days (Figure 3A). Due to the dramatic reduction in intact tissue, absolute liver weights and DNA content per liver were significantly decreased to 48 and 56% on day 4, respectively (Figure 3C).

While GLDH levels returned rapidly to pretreatment levels, the apoptotic activity remained elevated throughout the 31.5 days of observation (Figure 3A).

Regeneration of the liver

Regeneration of the liver started 48 h after NNM, as indicated by 10-fold increased replicative DNA synthesis (Figure 3B). As a result, total hepatic DNA content and absolute liver weights were back to their original level 24 days after NNM (Figure 3C). Rates of replication and apoptosis were still elevated at day 31.5, indicating that cell turnover was increased for at least 1 month after NNM (Figure 3A).

G+ single cells and multicellular foci after NNM treatment in histological sections (2D data)

Before treatment few G+ cells could be detected. After NNM G+ single cells increased dramatically in number reaching a maximum of ~150/cm^2 section area at day 13 (Figures 2 and 4A). The increase in the number of lesions consisting of 2, 3 and more G+ cells per cross section was less steep, with maxima at days 13 and 17. Thereafter, numbers of G+ single cells per cm^2 as well as of lesions <5 G+ cells per cross section declined. The number of G+ single cells dropped to one third of the maximum on day 34.5 (53/cm^2) and later to one fifth on day 107.5 post-treatment (Figure 4A). Lesions consisting of 2 or 3–5 G+ cells also leveled off to one third to one fifth of the peak value. The mean number of all lesions also slowly decreased to one third of the maximal value (200.2 ± 62.4/cm^2 at day 13.5 versus 60.5 ± 26/cm^2 at day 107.5, $P < 0.01$ according to Wilcoxon's test). A similar finding was reported by Satoh *et al*. (46).

Stereological estimates of G+ single cells and multicellular foci (3D projections)

In the present study many of the small G+ foci did not exhibit a spherical shape as assumed in previous modeling studies. As an example, Figure 2 shows a clone consisting of 6 G+ cells. In the extreme case, up to 11 G+ cells formed a chain-like row in two dimensions. Therefore, a novel stereological method was used which explicitly considers the composite nature and random shape of the cellular clones studied here (for details see Materials and methods). The computed number of G+ single cells and lesions per cm^2 agree well with the experimentally observed number, as shown in Table I.

The estimated 3D clone numbers were adjusted for total liver mass and were expressed per liver (Figure 4B). Both 2D data and 3D projections revealed three different phases after NNM administration. Phase I, lasting from day 0 to day 14 post-NNM, reflects the continuous appearance of G+ single cells and their development to multicellular foci. Phase II, lasting from day 14 to day 28, is characterized by regression of the number of G+ cell clones and loss of constituent cells. Due to the increase in liver mass after the first 2 weeks the decrease in G+ single cells and G+ lesions per liver was less pronounced than apparent on histological sections. In phase III, from day 28 onwards, the numbers of G+ single cells and of multicellular foci appeared to stabilize and an increase in larger foci was observed.

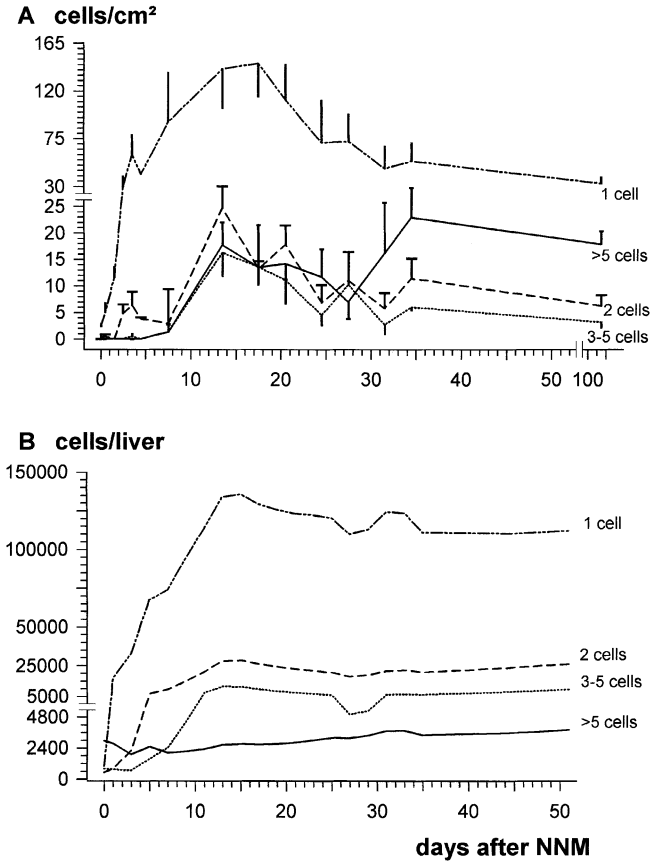

Fig. 4. (**A**) Kinetics of appearance of G+ single cells and G+ foci. Experimental data are expressed per cm^2 evaluated tissue sections between days 0 and 107.5 post-NNM treatment. G+ foci (>1 cell) were grouped into three different size classes according to the number of component cells per cross section (means ± SEM). (**B**) Calculated data expressed per liver between days 0 and 51 post-NNM treatment. 3D data were obtained by mathematical calculation; G+ lesions were divided into four different size classes according to the number of their component cells in three dimensions. Means are given.

Table I. Experimental and model-generated estimates of the occurrence of G+ single cells and G+ foci (to facilitate direct comparison experimental data were corrected for the relative change in liver volume)

Days after NNM	1 cell/cm^2 (exp)	1 cell/cm^2 (model)	>1 cell/cm^2 (exp)	>1 cell/cm^2 (model)
0.0	2.5 ± 2.0	2.0	1.3 ± 1.9	6.3
0.5	4.8 ± 3.5	6.1	0.4 ± 0.9	6.3
1.5	10.1 ± 4.6	14.3	0.0	6.6
2.5	18.2 ± 7.4	22.6	4.8 ± 3.3	7.3
3.5	33.0 ± 18.1	30.8	6.9 ± 7.7	8.3
4.5	34.6 ± 3.8	38.9	3.8 ± 0.5	9.6
7.5	64.2 ± 35.6	63.4	5.6 ± 3.5	5.5
13.5	105.0 ± 57.1	111.6	58.7 ± 5.2	36.1
17.5	115.1 ± 35.3	92.9	40.3 ± 24.8	28.1
20.5	94.9 ± 52.9	80.8	43.1 ± 17.1	23.5
24.5	69.0 ± 68.6	66.9	22.7 ± 21.3	18.7
27.5	78.6 ± 64.1	57.9	28.5 ± 24.9	16.1
31.5	58.8 ± 52.7	57.7	24.0 ± 26.5	17.0
34.5	58.9 ± 34.4	57.6	40.2 ± 16.6	17.6

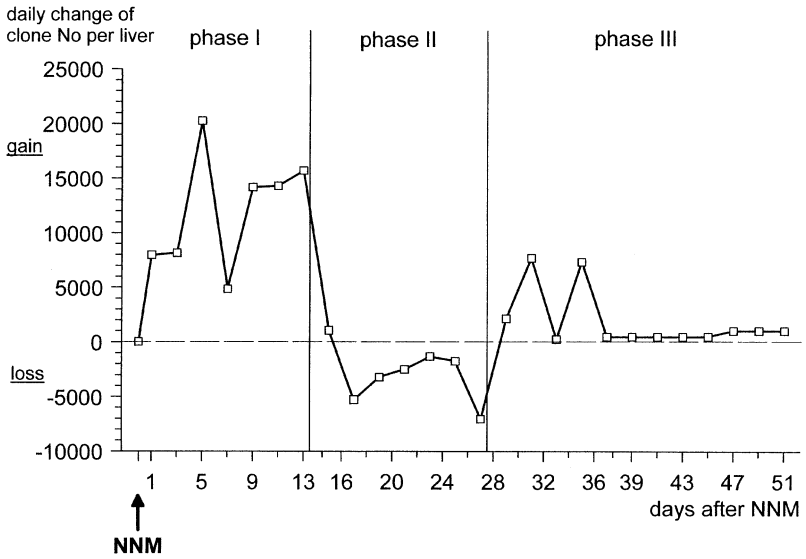

Fig. 5. Daily gain or loss of G+ clones per liver. 3D data were used to calculate the daily gain or loss of G+ cell clones in phases I, II and III post-NNM treatment.

Rate of formation of G+ cell clones

Using the maximum likelihood estimates of the growth model the number of cells initiated per liver per day and the expected number of clones per liver were computed (see Appendix). According to these estimates, ~5200 clones were present in the liver at day 0. Between days 1 and 14 after NNM ~171 000 new clones developed (mean rate per liver per day = 12 200); the total clone number decreased by ~42 200 (–23.9%) in phase II. In phase III the total number of G+ clones increased again, leading to the appearance of 11 350 new clones until day 51 (493 clones/liver/day). All phases together resulted in a net gain of ~140 150 G+ clones in the organ (for data per day see Figure 5). Due to the overwhelming numerical predominance of single G+ cells, gain or loss of all G+ cells, including those from larger foci, were within a similar range (approximate numbers: phase I, +231 000 G+ cells; phase II, –57 000 G+ cells; phase III, +52 000 G+ cells; total gain 226 000 G+ cells).

Furthermore, the 3D size estimates imply that by day 51 post-NNM 23.9% of the G+ single cells appearing after NNM had formed 2 cell foci and only 0.3% of the foci had grown into foci containing >5 cells.

DNA synthesis in single G+ cells and their precursors

DNA replication, which was determined by [^{3}H]thymidine incorporation 36 h before death, was assayed on histological sections. At multiple time points after NNM LIs of single G+ cells were generally low and were consistently less than of G– cells and of G+ cells in lesions of ⩾2 cells (Figure 6, upper panel). This suggests that the precursors of single G+ cells had a low rate of DNA synthesis 36 h before observation (killing). A similar result was seen when [^{3}H]thymidine was injected only 12 h before death (Table II).

Next we studied whether the appearance of single G+ cells after NNM depends on preceding DNA replication. LIs of single G+ cells were specifically determined in phase I 36 h after [^{3}H]thymidine injection, starting at the time of NNM application. As shown in Table III, LIs of single cells and hence of their precursors were much lower than expected if DNA replication in the precursors were required for the subsequent formation of G+ single cells. This implies that the steep increase in single G+ cells in the first days after NNM does not depend on preceding DNA replication.

We also determined DNA replication 2 h after [^{3}H]thymidine application to assess LI of G+ single cells directly, rather than of their precursors. Under these conditions LI of G+ single cells also ranged considerably below that of G– cells and G+ foci (Table II). This suggests that replication to a 2-cell clone occurs considerably less frequently than replication of G– cells and of cells in G+ foci.

For stereological reasons some G+ cells appearing as single in histological sections (2D) are actually part of G+ foci with ⩾2 cells. We therefore determined the true percentage of [^{3}H]thymidine-labeled single G+ cells by 3D reconstruction in serial sections: 73% of all but only 26% of the labeled G+ single cells in two dimensions were truly single in three dimensions (Table IV). This result indicates that the low LI of single G+ cells reported above are still overestimates. True rates of DNA synthesis of single G+ cells and of their precursors are even lower and may, on average, be only ~25% of rates calculated from histological counts.

Since the detection of GST-P in the apoptotic stage is not reliable (see Materials and methods), the number of G+ single cells undergoing apoptosis could not be determined experimentally.

DNA synthesis and apoptosis in G+ foci

In G+ mini-foci the measured LIs for cell replication and AIs for apoptosis were initially high and then decreased in the course of the experiment (Figure 6). Replication was ~3- to 5-fold higher in the foci than in the surrounding normal tissue, which was seen after a 2, 12 and 36 h lag between [^{3}H]thymidine injection and death (Figure 6 and Table II). Rates of apoptosis in G+ foci were also 3- to 5-fold above the level of normal hepatocytes, indicating elevated cell turnover in the first stages of hepatocarcinogenesis (Figure 6).

Estimation of cell kinetic parameters of initiated cells by mathematical analysis

The stochastic growth model combined with the stereological procedure served to estimate the division rate (α) and death rate (β) of the G+ lesions. The growth model assumes

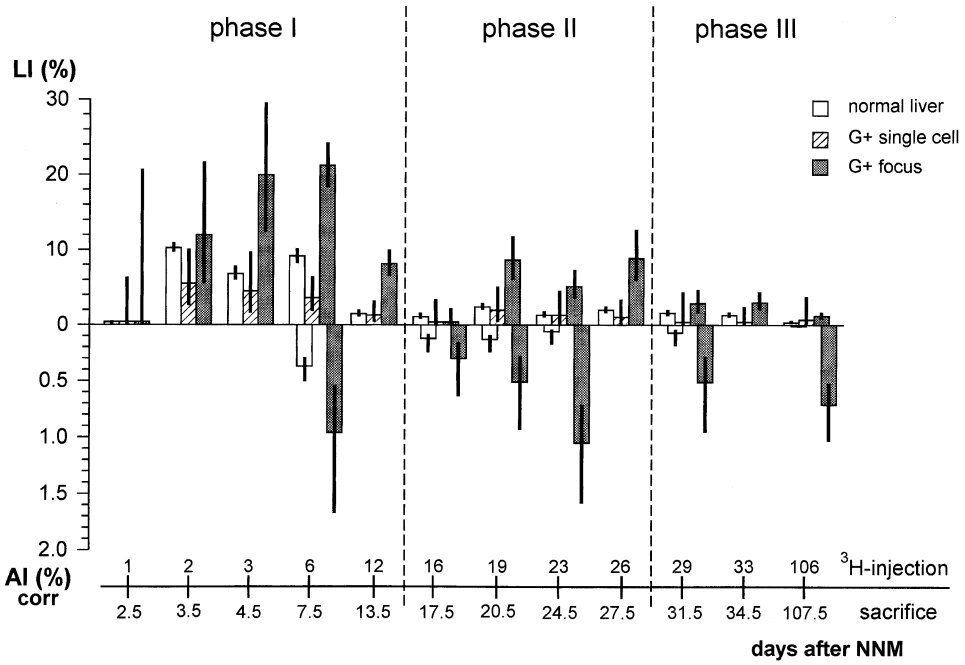

Fig. 6. Cell replication and apoptosis in early hepatocarcinogenesis. DNA synthesis (LI%) was determined separately in G– hepatocytes, in single G+ cells and in lesions of 2, 3–5 and >5 G+ cells. Since no differences in LIs of lesions with ⩾2 cells were apparent (data not shown), the subpopulations were combined. The same procedure was followed for the determination of apoptosis (AI%corr), with the exception that AI could not be determined before day 7.5 post-NNM and in single cells at all time points. For the method for correction of AI (AI_{corr}) see Materials and methods. Note that [^{3}H]thymidine was injected 36 h before killing (see abscissa). For each time point LI was determined on average in 178 nuclei of G+ single cells and in 829 nuclei of G+ foci, whereas a mean of 2392 cells in G+ foci was screened for AI. Vertical lines indicate confidence intervals; no overlap indicates a significant difference at the 95% level. Note the difference in the scales of the ordinates.

Table II. LI of G– hepatocytes, G+ single cells and G+ foci (⩾2 cells) in two dimensions after different time intervals between label injection at day 19 post-NNM and killing

Interval between injection and death	LI		
	G– cells (95% CI)	G+ single cells (95% CI)	G+ foci (95% CI)
36 h	2.39 (2.08–2.79) n = 8000	1.94 (0.5–4.96) n = 192	8.63 (6.12–11.65) n = 440
12 h	3.87 (3.49–4.35) n = 8000	1.85 (0.36–5.35) n = 162	7.32 (5.82–9.09) n = 1024
2 h	1.52 (1.29–1.85) n = 9000	0.68 (0.18–1.73) n = 586	2.35 (1.63–3.32) n = 1402

Table III. LI of single G+ cells in phase I after NNM

Day of		LI (%) experimental	New G+ single cells formed per day/total G+ single cells	Calculated % of G+ single cells labeled per day
Label injection	Killing			
0	1.5	0 (n = 12)	12 200/18 400	66.3
1	2.5	0 (n = 57)	12 200/30 600	39.9
2	3.5	5.5 (n = 176)	12 200/42 800	28.5
3	4.5	4.5 (n = 133)	12 200/55 000	22.2
6	7.5	3.6 (n = 336)	12 200/91 600	13.3
12	13.5	1.3 (n = 382)	12 200/164 800	7.4

LIs were experimentally determined. n, number of single cells evaluated. We also calculated the expected number of labeled G+ single cells based on the assumption that the appearance of G+ cells requires preceding DNA replication. The number of 12 200 new G+ cells formed in the liver per day and per total experimental period was taken from the results.

that all G+ cells divide or disappear with the same rate regardless of clone size. Due to the overwhelming numerical predominance of G+ single cells in the data, the estimated α_2 and β_2 values represent mainly single cells. Therefore, lesions of >1 G+ cell were subjected to a separate analysis to compute α_3 and β_3. Table V compares estimated α and β values with experimentally derived rates for cell division and cell death among all G+ lesions, including G+ single cells, and among lesions with at least 2 G+ cells.

The maximum likelihood estimates of the cell division rate α_2, which also represents the daily rate of single cells entering the 2 cell stage, was 4% in phase I and dropped to 0.5% in

phases II and III (Table V). These estimates are in good agreement with the experimental LI in G+ single cells and with the observation that labeled G+ cells appearing single in two dimensions arose mainly from division into 2 G+ cells. Consistent with the experimental data, α_3 was dramatically higher than α_2, indicating enhanced cell replication in lesions of >1 G+ cell.

Estimation of death rates revealed the highest β_2 and β_3 values of G+ cells in regression phase II, when G+ cells disappear at a rate of ~6 or 20% per day, respectively, leading to a net loss of G+ cells ($\beta_2 > \alpha_2$; $\beta_3 > \alpha_3$). In phases I and III, however, the model predicts a net gain of G+ cells ($\alpha_2 > \beta_2$; $\alpha_3 > \beta_3$), which is consistent with the experimental data.

Discussion

The present study shows that G+ single cells emerged in rat liver during the ~2 weeks after NNM treatment. A subfraction of these putatively initiated cells developed into G+ preneoplasias. A considerable number of the cells, however, underwent apoptosis, leading to extinction of single G+ cells and to decreased sizes of G+ multicellular clones. Implications and hypotheses resulting from our findings are discussed below.

Clonal evolution of hepatocarcinogenesis

The consecutive development of G+ single cells into G+ foci consisting of 2, 3–5 and >5 cells (Figure 4) supports the concept that liver preneoplasias are of monoclonal origin and that expression of the G+ phenotype is heritable by daughter cells. Mathematical analysis of the experimental data confirmed the clonal nature of liver preneoplasias and the persistent phenotype of the component cells. This also agrees with previous reports, e.g. homogeneous expression of isoenzymes in early preneoplasia (11,47).

Is DNA synthesis necessary for subsequent formation of G+ single cells?

Theoretically, G+ single cells may emerge from G– cells without preceding DNA replication or via asymmetrical division into a G– and a G+ cell. In the latter case expression of the G+ phenotype in one of the two daughter cells might follow immediately after DNA replication or after a certain time interval. If expression of the G+ phenotype was preceded by DNA synthesis a high proportion of G+ single cells, emerging in the first few days after NNM, should be labeled. [^{3}H]thymidine was injected 0, 24 and 48 h after NNM treatment. At killing 36 h after label injection the G+ single cells newly formed within 24 h should carry the label. In sharp contrast to this prediction, LIs of G+ single cells in two dimensions were extremely low at death, i.e. 0% on days 1.5 and 2.5 and ~4% on the following days (Figure 6 and Table III). Furthermore, after stereological reconstruction only 26% of the labeled G+ single cells in histological sections (2D) turned out to be a true single G+ cell in three dimensions (Table IV). Thus, no more than ~1% of the G+ single cells seem to replicate DNA within 36 h of their formation.

In conclusion, a high proportion of G+ single cells, at least in the first days after NNM treatment, are formed without preceding DNA synthesis. These findings appear to contradict the classical concept of initiation, i.e. that the generation of an 'initiated' phenotype requires a genetic alteration which is fixed by replication. Since the molecular mechanisms of induction of the G+ phenotype are not known, the appearance of G+ hepatocytes could be due to epigenetic rather than genetic events.

Experimental and mathematical determination of DNA synthesis in G+ single cells and small G+ foci

In several experimental approaches (see Figure 6 and Tables II and III) replication of G+ single cells was found to be considerably lower than in lesions consisting of >1 G+ cell. Independent mathematical estimates confirmed the low rate of single cells entering the 2 cell stage (Table V). The reasons for this finding are unclear. It appears unlikely that G+ single cells suffer from the genotoxic and cytotoxic effects of NNM, since a low replication rate was still observed on day 107.5 post-NNM treatment. Rather, it may be an inherent property of G+ single cells to be less prone to proliferation than small G+ clones.

The model also confirmed an elevated replication rate in multicellular lesions. This is further evidence for altered growth regulation from the very beginning of hepatocarcinogenesis onwards.

Table IV. 3D reconstruction of G+ lesions appearing as single G+ cells in two dimensions

Days after NNM	2D No. of single G+ cells analyzed	3D True clone size		
		1 G+ cell	2 G+ cells	>2 G+ cells
(A) 13.5	n = 61	45 (74%)	14 (23%)	2 (3%)
34.5	n = 64	47 (74%)	11 (17%)	6 (9%)
107.5	n = 29	21 (72%)	7 (24%)	1 (4%)
Sum	n = 154	113 (73%)	32 (21%)	9 (6%)
(B) 7.5	n = 15	2 (13%)	12 (80%)	1 (7%)
13.5	n = 10	4 (40%)	6 (60%)	0 (0%)
34.5	n = 2	1 (50%)	1 (50%)	0 (0%)
Sum	n = 27	7 (26%)	19 (70%)	1 (4%)

For each time point 20 serial sections ~3 μm thick were used, stained for GST-P and processed for autoradiography. The interval between [^{3}H]thymidine injection and killing was 36 h. In (A) G+ lesions were evaluated independent of whether they were labeled or not; (B) indicates the 3D size of lesions appearing as labeled G+ single cells in two dimensions.

Table V. Experimental and calculated rates of cell birth and death of initiated G+ cells

	LI (%)		α_2 (%) (95% CI)	α_3 (%) (95% CI)	AI_{corr} (%) >1 cell	β_2 (%) (95% CI)	β_3 (%) (95% CI)
	1 cell	>1 cell					
Phase I	2.8	14.0	4.2 (3.1–5.2)	22.7 (19.2–26.9)	2.3	0.0	0.0 (0.0–9.5)
Phase II	1.1	6.1	0.5 (0.0–2.5)	12.8 (3.6–21.6)	3.4	6.2 (4.6–8.6)	19.1 (7.7–29.6)
Phase III	0.02	2.5	0.5 (0.0–2.5)	12.8 (3.6–21.6)	1.3	0.2 (0.0–5.5)	0.0 (0.0–90.0)

Experimental data on LI and AI_{corr}, shown in Figure 6, were used to calculate means for phases I–III. Rates of cell birth α_2 and of cell death β_2 are maximum likelihood estimates from the stochastic growth model (for details see Materials and methods).

Experimental and mathematical determination of apoptosis in G+ single cells and small G+ foci

In the stochastic growth model β does not distinguish between death of G+ cells and disappearance of the G+ phenotype. Comparison of data determined experimentally and mathematically revealed that in phases I and III β values and the percentage of ABs were within a similar range; thus β represents mainly loss of G+ cells, at least under the present experimental conditions (Table V).

The highest apoptotic activities of G+ cells were found in regression phase II. For this phase the model predicts that G+ single cells die at a rate of ~0.06/day (Table V). With current experimental procedures it is not possible to detect apoptotic events associated with the death of single G+ cells. Thus, a direct comparison between the mathematical and experimental data is not feasible. In addition, the molecular mechanisms of the appearance of single G+ hepatocytes are not known and could be due to unstable epigenetic rather than genetic changes. Then transient expression only of the G+ phenotype in single cells could be the cause of the disappearance of G+ cells at the later time points of the experiment.

In phase II the mathematically estimated death rate of 0.20 for G+ cells in multicellular foci (β_3) exceeds the experimentally determined rate of ~0.035 (Table V). This discrepancy may, at least in part, be due to a sampling bias, i.e. large lesions with a probably lower apoptotic activity have a higher probability of being hit by random cuts than small lesions with a presumably high apoptotic activity. Furthermore, there was considerable heterogeneity in the cell kinetic parameters in the foci.

Changes in replication and death of G+ cells in the course of liver regeneration after NNM

Both cell replication and cell death by apoptosis determine the fate of G+ clones. In any case, in phase II β values exceeded α values, resulting in a net loss of G+ cells. Conversely, in phases I and III the model predicts a net gain of G+ cells, i.e. $\alpha_2 > \beta_2$; $\alpha_3 > \beta_3$. These independent calculations are consistent with our experimental data (Table V).

The change in rates of replication and death of G+ cells observed in phases I–III may reflect alterations in the concentrations of growth factors in the liver (48,49). In phase I regeneration signals, released in response to severe damage to the liver, may act on G+ cells and are probably responsible for the dramatic expansion of all G+ clones. In phase II regeneration of the liver and release of growth factors slows down. This probably results in deprivation of G+ cells of factors required for survival and/or growth. As a result, G+ clones stop growing and lose component cells.

Similar phenomena may occur in virus-induced hepatocarcinogenesis in humans, which is further enhanced by repeated aflatoxin B1 or alcohol intoxication. It appears that sustained cell damage or inflammatory responses in the liver release growth-promoting stimuli that are necessary for the development of (pre)neoplasias (50).

Characteristics of initiated cells

Elevated cell turnover is one of the hallmarks of the advanced stages of carcinogenic development. (Pre)neoplastic lesions exhibit enhanced sensitivity towards growth regulating factors which results in preferential growth or regression of the lesion (27,51). The present study shows that G+ single cells do not meet this criterion and that this important characteristic does not become manifest before lesions consist of at least 2 G+ cells. Thus early hepatocarcinogenesis seems to involve a kind of intermediary cell population that gives rise to a cell population undergoing preferential expansion or regression. It would be important to elucidate the mechanisms regulating this complex development. Then it might become feasible to induce preferential loss of initiated cells and thereby to antagonize the process of tumorigenesis at the very beginning.

Preferential growth or elimination of G+ cells

The findings described above allow for the following conclusions, as schematically depicted in Figure 7. In healthy tissues a low cell turnover (α_1, β_1) protects against dramatic alterations in cell numbers. Initiation (μ_1) generates persistent and irreversible cellular changes leading to altered α_2 and β_2 values in G+ single cells. Elevated cell turnover (α_3 and β_3) becomes evident in lesions of >1 G+ cells, which renders G+ cells more sensitive to induction of both proliferation and extinction. An elevation of β may result in two different biological consequences. (i) The smaller the G+ clone the greater the probability of its complete elimination. By this mechanism the biological consequences of initiation may be reversed. Evidence for at least partial elimination of G+ clones was gained in phase II of the present study, but also in previous studies on food restriction or withdrawal of tumor-promoting agents (27,40). Thus, the early stages of cancer may be extinguished under appropriate conditions. (ii) The larger the G+ clone the smaller the probability of complete extinction. The G+ clone will be reduced in size but will not be eradicated, which reverses the effect of tumor promotion.

In conclusion, putatively initiated hepatocytes, from the 2-cell stage onwards, exhibit accelerated turnover and preferential growth or regression, as known for large foci, adenomas and carcinomas. Thus altered regulation of growth control becomes manifest from the very beginning of hepatocarcinogenesis onwards.

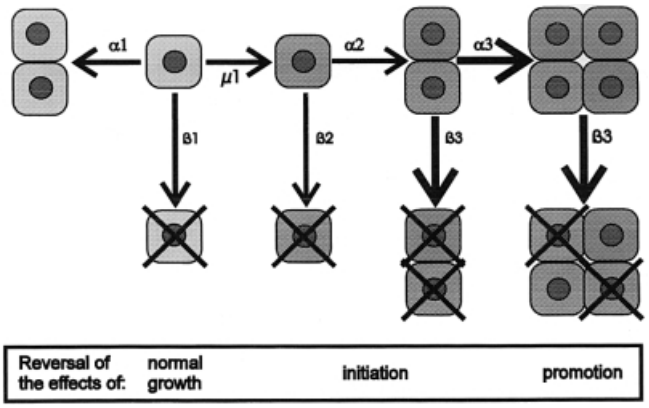

Fig. 7. Effects of cell birth and cell death on the early stages of hepatocarcinogenesis. Normal cells, light grey; initiated cells, dark grey; μ1, daily rate of initiation; α, daily rate of cell birth; β, daily rate of cell death. The net growth rate of cell populations is principally determined by the difference between birth rates α and death rates β (= α – β). Initiated cells are characterized by altered rates of cell birth (α_2, α_3) and of cell death (β_2, β_3); clonal expansion is favoured if, for example, $(\alpha_3 - \beta_3) > (\alpha_1 - \beta_1)$. The probability of a cell being extinguished is determined by the ratio of birth and death rates (= β/α) and is inversely proportional to the number of component cells in a given tissue (25). Thus single cells have the highest probability of being extinguished. Extinction of single cells or foci may reverse the biological consequence of tumor initiation. Reduction in clone size will antagonize the effect of tumor promotion.

Acknowledgements

The excellent technical assistance of K.Bukowska, M.Käfer and H.Koudelka is gratefully acknowledged. This study was supported by Herzfelder'sche Familienstiftung. We also thank Nycomed Austria for financial support of this study, which was performed within the training program 'Hochschullehrgang für Toxikologie' at the University of Vienna.

References

1. Farber,E. and Cameron,R. (1980) The sequential analysis of cancer development. *Adv. Cancer Res.*, **31**, 125–226.
2. Appel,K.E., Fürstenberger,G., Hapke,H.J., Hecker,E., Hildebrandt,A.G., Koransky,W., Marks,F., Neumann,H.G., Ohnesorge,F.K. and Schulte-Hermann,R. (1990) Chemical cancerogenesis: definitions of frequently used terms. *J. Cancer Res. Clin. Oncol.*, **116**, 232–236.
3. Pitot,H.C. and Dragan,Y.P. (1991) Facts and theories concerning the mechanisms of carcinogenesis. *FASEB J.*, **5**, 2280–2286.
4. Satoh,K., Kitahara,A., Soma,Y., Inaba,Y., Hatayama,I. and Sato,K. (1985) Purification, induction and distribution of placental glutathione transferase: a new marker enzyme for preneoplastic cells in the rat chemical hepatocarcinogenesis. *Proc. Natl Acad. Sci. USA*, **82**, 3964–3968.
5. Sato,K. (1989) Glutathione transferases as markers for preneoplasia and neoplasia. *Adv. Cancer Res.*, **52**, 205–255.
6. Moore,M.A., Nakagawa,K., Satoh,K., Ishikawa,T. and Sato,K. (1987) Single GST-P positive liver cells—putative initiated hepatocytes. *Carcinogenesis*, **8**, 483–486.
7. Gopolan,P., Tsuji,K., Lehman,K., Kimura,M., Shinozuka,H., Sato,K. and Lotlikar,P.D. (1993) Modulation of aflatoxin B1-induced glutathione S-transferase placental form positive hepatic foci by pretreatment of rats with phenobarbital and buthionine sulfoximine. *Carcinogenesis*, **14**, 1469–1470.
8. Qin,G., Gopalan-Kriczky,P., Su,J., Ning,Y. and Lotlikar,P.D. (1997) Inhibition of aflatoxin B1-induced initiation of hepatocarcinogenesis in the rat by green tea. *Cancer Lett.*, **112**, 149–154.
9. Bauer-Hofmann,R., Klimek,F., Buchmann,A., Muller,O., Bannasch,P. and Schwarz,M. (1992) Role of mutations at codon 61 of the c-Ha-ras gene during diethylnitrosamine-induced hepatocarcinogenesis in C3H/He mice. *Mol. Carcinog.*, **6**, 60–67.
10. Baba,M., Yamamoto,R., Iishi,H. and Tatsuta,M. (1997) Ha-ras mutations in N-nitrosomorpholine-induced lesions and inhibition of hepatocarcinogenesis by antisense sequences in rat liver. *Int. J. Cancer*, **72**, 815–820.
11. Dragan,Y.P., Peterson,J. and Pitot,H.C. (1993) Comparison of hepatocyte phenotypes at the glutathione transferase and albumin loci in Sprague–Dawley and Nagase analbuminemic rats and F1 progeny after initiation and promotion. *Carcinogenesis*, **14**, 1313–1319.
12. Pitot,H.C., Dragan,Y.P., Teeguarden,J., Hsia,S. and Campbell,H. (1996) Quantitation of multistage carcinogenesis in rat liver. *Toxicol. Pathol.*, **24**, 119–128.
13. Druckrey,H. (1967) Quantitative aspects in chemical carcinogenesis. In Truhaut,R. (ed.) *Potential Carcinogenic Hazards From Drugs*, UICC Monograph. Springer, Berlin, Germany, Vol. 7, pp. 1–14.
14. Moolgavkar,S.H. and Knudson,A.G.,Jr (1981) Mutation and cancer: a model for human carcinogenesis. *J. Natl Cancer Inst.*, **66**, 1037–1052.
15. Thorslund,T.W., Brown,C.C. and Charnley,G. (1987) Biologically motivated cancer risk models. *Risk Anal.*, **7**, 109–119.
16. Dewanji,A., Venzon,D.J. and Moolgavkar,S.H. (1989) A stochastic two-stage model for cancer risk assessment. II. The number and size of premalignant clones. *Risk Anal.*, **9**, 179–187.
17. Pitot,H.C., Neveu,J., Hully,J.R., Rizvi,T.A. and Campbell,H. (1990) Multistage hepatocarcinogenesis in the rat as a base for models of risk assessment of carcinogenesis. In Moolgavkar,S.H. (ed.) *Scientific Issues in Quantitative Cancer Risk Assessment*. Birkhauser, Boston, MA, pp. 69–95.
18. Travis,C.C., McClain,T.W. and Birkner,P. (1991) Diethylnitrosamine-induced hepatocarcinogenesis in rats: a theoretical study. *Toxicol. Appl. Pharmacol.*, **109**, 289–304.
19. Kopp-Schneider,A. (1992) Birth-death processes with piecewise constant rates. *Statist. Probabil. Lett.*, **13**, 121–127.
20. Kramer,D.A. and Conolly,R.B. (1997) Computer simulation of clonal growth cancer models. I. Parameter estimation using an iterative absolute bisection algorithm. *Risk Anal.*, **17**, 115–126.
21. Fullman,R.L. (1953) Measurement of particle sizes in opaque bodies. *Trans. AIME*, **197**, 447–452.
22. Saltykov,S. (1967) The determination of the size distribution of particles in an opaque material from a measurement of the size distribution of their sections. In Elias,H. (ed.) *Proceedings of the Second International Congress of Stereology.* Springer, Berlin, Germany, pp. 153–173.
23. Campbell,H.A., Pitot,H.C., Potter,V.R. and Laishes,B.A. (1982) Application of quantitative stereology to the evaluation of enzyme-altered foci in rat liver. *Cancer Res.*, **42**, 465–472.
24. de Gunst,M.C.M. and Luebeck,E.G. (1998) A method for parametric estimation of the number and size distribution of cell clusters from observations in a section plane with an application to preneoplastic minifoci in rat liver. *Biometrics*, **54**, 100–112.
25. Moolgavkar,S.H., Luebeck,G., De Gunst,M., Port,R.E. and Schwarz,M. (1990) Quantitative analysis of enzyme altered foci in rat hepatocarcinogenesis experiments. *Carcinogenesis*, **11**, 1271–1278.
26. Schulte-Hermann,R., Ohde,G., Schuppler,J. and Timmermann-Trosiener,I. (1981) Enhanced cell proliferation of putative preneoplastic cells in rat liver following treatment with the tumor promoters phenobarbital, hexachlorocyclohexane, steroid compounds and nafenopin. *Cancer Res.*, **41**, 2556–2562.
27. Grasl-Kraupp,B., Ruttkay-Nedecky,B., Müllauer,L., Taper,H., Huber,W., Bursch,W. and Schulte-Hermann,R. (1997) Inherent increase of apoptosis in liver tumors: implications for carcinogenesis and tumor regression. *Hepatology*, **25**, 906–911.
28. Rotstein,J., Sarma,D.S. and Farber,E. (1986) Sequential alterations in growth control and cell dynamics in rat hepatocytes in early precancerous steps in hepatocarcinogenesis. *Cancer Res.*, **46**, 2377–2385.
29. Bursch,W., Lauer,B., Timmermann-Trosiener,I., Barthel,G., Schuppler,J. and Schulte-Hermann,R. (1984) Controlled death (apoptosis) of normal and putative preneoplastic cells in rat liver following withdrawal of tumor promoters. *Carcinogenesis*, **5**, 453–458.
30. Bursch,W., Taper,H.S., Lauer,B. and Schulte-Hermann,R. (1985) Quantitative histological and histochemical studies on the occurrence and stages of controlled cell death (apoptosis) during regression of rat liver hyperplasia. *Virchows Arch. B Cell Pathol.*, **50**, 153–166.
31. Schulte-Hermann,R., Timmermann-Trosiener,I., Barthel,G. and Bursch,W. (1990) DNA synthesis, apoptosis and phenotype expression as determinants of growth of altered foci in rat liver during phenobarbital promotion. *Cancer Res.*, **50**, 5127–5135.
32. Swann,P.F., Graves,R.J. and Mace,R. (1987) International Commission for Protection against Environmental Mutagens and Carcinogens. Effect of ethanol on nitrosamine metabolism and distribution. Implications for the role of nitrosamines in human cancer and for the influence of alcohol consumption on cancer incidence. *Mutat. Res.*, **186**, 261–267.
33. Bartsch,H., Ohshima,H., Pignatelli,B. and Calmels,S. (1992) Endogeneously formed N-nitroso compounds and nitrosating agents in human cancer etiology. *Pharmacogenetics*, **2**, 272–277.
34. Wesierska-Gadek,J., Bugajska-Schretter,A., Löw-Baselli,A. and Grasl-Kraupp,B. (1999) Cleavage of poly(ADP-ribose) transferase during p53-independent apoptosis in rat liver after treatment with N-nitrosomorpholine and cyproterone acetate. *Mol. Carcinog.*, **24**, 263–275.
35. Schwarz,M., Bannasch,P. and Kunz,W. (1983) The effect of pre- and post-treatment on the extent of gamma-glutamyl transpeptidase positive foci induced in rat liver by N-nitrosomorpholine. *Cancer Lett.*, **21**, 17–21.
36. Schroter,C., Parzefall,W., Schroter,H. and Schulte-Hermann,R. (1987) Dose-response studies on the effects of α-, β- and γ-hexachlorocyclohexane on putative preneoplastic foci, monooxygenases and growth in rat liver. *Cancer Res.*, **47**, 80–88.
37. Parzefall,W., Schuppler,J., Barthel,G., Meyer-Rogge,B. and Schulte-Hermann,R. (1990) Toxicological studies on a benzofurane derivative. I. A comparative study with phenobarbital on rat liver. *Toxicol. Appl. Pharmacol.*, **106**, 482–499.
38. Schulte-Hermann,R. (1977) Two-stage control of cell proliferation induced in rat liver by α-hexachlorocyclohexane. *Cancer Res.*, **37**, 166–171.
39. Grasl-Kraupp,B., Waldhör,T., Huber,W. and Schulte-Hermann,R. (1993) Glutathione *S*-transferase isoenzyme patterns in different subtypes of enzyme-altered rat liver foci treated with the peroxisome proliferator nafenopin or with phenobarbital. *Carcinogenesis*, **14**, 2407–2412.
40. Grasl-Kraupp,B., Bursch,W., Ruttkay-Nedecky,B., Wagner,A., Lauer,B. and Schulte-Hermann,R. (1994) Food restriction eliminates preneoplastic cells through apoptosis and antagonizes carcinogenesis in rat liver. *Proc. Natl Acad. Sci. USA*, **91**, 9995–9999.
41. Schulte-Hermann,R. (1974) Induction of liver growth by xenobiotic compounds and other stimuli. *Crit. Rev. Toxicol.*, **3**, 97–115.
42. Jack,E.M., Bentley,P., Bieri,F., Muakkassah-Kelly,S.F., Stäubli,W., Suter,J., Waechter,F. and Cruz-Orive,L.M. (1990) Increase in hepatocyte and nuclear volume and decrease in the population of binucleated cells in preneoplastic foci of rat liver. A stereological study using the nucleator method. *Hepatology*, **11**, 286–297.
43. Wicksell,D.S. (1925) The corpuscle problem, part I. *Biometrika*, **17**, 87–97.

44. Press,W.H., Flannery,B.P., Teukolsky,S.A. and Vetterling,W.T. (1986) *Numerical Recipes: The Art of Scientific Computing*. Cambridge University Press, Cambridge, UK.
45. Venzon,D.J. and Moolgavkar,S.H. (1988) A method for computing profile-likelihood-based confidence intervals. *Appl. Stat.*, **37**, 87–94.
46. Satoh,K., Hatayama,I., Tateoka,N., Tamai,K., Shimizu,T., Tatematsu,M., Ito,N. and Sato,K. (1989) Transient induction of single G+ hepatocytes by DEN. *Carcinogenesis*, **10**, 2107–2111.
47. Pitot,H.C. (1990) Altered hepatic foci: their role in murine hepatocarcinogenesis. *Annu. Rev. Pharmacol. Toxicol.*, **30**, 465–500.
48. Fausto,N. and Webber,E.M. (1993) Mechanisms of growth regulation in liver regeneration and hepatic carcinogenesis. In Boyer,J.L. and Ockner,R.K. (eds) *Progress in Liver Diseases*. Saunders, Philadelphia, PA, pp. 115–137.
49. Michalopoulos,G.K. and DeFrances,M.C. (1997) Liver regeneration. *Science*, **276**, 60–66.
50. Fu-Sun,Y., Yu,M.C., Mo,C.-C., Luo,S., Tong,M.J. and Henderson,B.E. (1989) Hepatitis B virus, aflatoxins and hepatocellular carcinoma in southern Guangxi, China. *Cancer Res.*, **49**, 2506–2509.
51. Schulte-Hermann,R., Bursch,W. and Grasl-Kraupp,B. (1995) Active cell death (apoptosis) in liver biology and disease. In Boyer,J.L. and Ockner,R.K. (eds) *Progress in Liver Diseases*. Saunders, Philadelphia, PA, pp. 1–35.
52. Luebeck,E.G., Moolgavkar,S.H., Buchmann,A. and Schwarz,M. (1991) Effects of polychlorinated biphenyls in rat liver: quantitative analysis of enzyme altered foci. *Toxicol. Appl. Pharmacol.*, **111**, 469–484.
53. Luebeck,E.G., Grasl-Kraupp,B., Timmermann-Trosiener,I., Bursch,W., Schulte-Hermann,R. and Moolgavkar,S.H. (1995) Growth kinetics of enzyme altered liver foci in rats treated with phenobarbital or α-hexachlorocyclohexane. *Toxicol. Appl. Pharmacol.*, **130**, 304–315.

Received December 30, 1999; revised March 21, 2000; accepted March 27, 2000

Appendix

The expressions for the size and number distribution of enzyme-altered foci that were used for the present analysis are generalizations of the formulae used in previous analyses (for details see refs 25,52,53). A derivation of these expressions within the framework of the two-stage model of carcinogenesis can be found in Dewanji *et al.* (16). For piecewise constant parameters the number and size distribution formulae can be integrated and expressed in closed form (19). Here, a brief summary of the basic results, for the case of an arbitrary number of intervals with (piecewise) constant parameters, is given. The choice of notation and the particular choice of auxiliary parameters is motivated by simplicity and ease of programming.

Assume k intervals $I_i = [t_i, t_{i+1}]$, $(i = 1,\text{K}, k)$ with $t_1 = 0$ and $t_{k+1} = t$. Let the cell division rate be α_i, the cell death rate be β_i and the initiation rate (per unit volume) be ν_i on the ith interval I_i. Define the functions

$$p_m^{(i)} = 1/m\{[\alpha_i - \tilde{\alpha}_i g_i(t_i, t_{i+1})]/[\alpha_i - \tilde{\beta}_i g_i(t_i, t_{i+1})]\}^m$$

with

$$g_i(t_i, t_{i+1}) \equiv \exp[-\delta_i(t_{i+1} - t_i)],\ \delta_i = \alpha_i - \beta_i.$$

The auxiliary rate variables $\tilde{\alpha}_i$ and $\tilde{\beta}_i$ can be obtained recursively from the hierarchy

$$\tilde{\alpha}_k = \alpha_k$$

$$\tilde{\alpha}_{k-1} = \alpha_{k-1} - \delta_{k-1}(\alpha_k - \tilde{\alpha}_k g_k)/\delta_k$$

$$\tilde{\alpha}_{k-2} = \alpha_{k-2} - \delta_{k-2}(\alpha_{k-1} - \tilde{\alpha}_{k-1} g_{k-1})/\delta_{k-1}$$

$$\text{M}$$

$$\tilde{\alpha}_1 = \alpha_1 - \delta_1(\alpha_2 - \tilde{\alpha}_2 g_2)/\delta_2$$

$$\text{Then, } \tilde{\beta}_i = \tilde{\alpha}_i - \tilde{\delta}_i \text{ with } \tilde{\delta}_i = \delta_i \prod_{j=i+1}^{k} g_j(t_j, t_{j+1}).$$

With these definitions the expected number of clones (per unit volume), EN_V, can be written as a sum over all time intervals prior to time t:

$$EN_V = \sum_{i=1}^{k} (\nu_i/\alpha_i)\ln\{[\alpha_i g_i^{-1}(t_i, t_{i+1}) - \tilde{\beta}_i]/[\alpha_i - \tilde{\beta}_i]\}$$

and the size distribution, p_m, as a sum (defining $\nu_0/\alpha_0 = 0$)

$$p_m = (1/EN_V)\sum_{i=1}^{k}[(\nu_i/\alpha_i) - (\nu_{i-1}/\alpha_{i-1})]p_m^{(i)}$$

Finally, the expected number of m cell clones (per unit volume) is simply $p_m EN_V$. In the case of a separate analysis of lesions of >1 G+ cells replace α_2 by α_3 and β_2 by β_3. Please note that in the Results time intervals 1, 2 and 3 are designated phases I–III.